(Received 4 January 2024, Accepted 23 January 2024, Scheduled 8 February 2024)

Circularly Polarized Double-Walled SIW Fractal Slot and Hexagonal Ring Slot Antenna Array for X-Band Satellite Applications

Mostafa Mahmoud Rabie[1, 2, *], Mohamed S. El-Gendy[3], A. R. Eldamak[2], Fawzy Ibrahim[4], and Hadia El-Henawy[2]

[1] *Electrical and Electronics Engineering Coventry University, Cairo, Egypt*
[2] *Electronics and Communications Engineering Department, Ain Shams University, Cairo, Egypt*
[3] *Electronics Research Institute, Cairo, Egypt*
[4] *Egyptian Academy for Engineering and Advanced Technology, Cairo, Egypt*

ABSTRACT: This paper presents a circularly polarized double wall substrate integrated waveguide (SIW) fractal slot antenna array designed for X-band satellite applications. The proposed antenna demonstrates a reflection coefficient, covering the frequency range from 7.3 GHz to 8.5 GHz. The antenna is circularly polarized with a 3-dB axial ratio bandwidth ranging from 7.88 GHz to 8.58 GHz. The antenna array exhibits a gain variation between 11 dBi and 12.51 dBi. Moreover, the proposed design achieves an efficiency of 89%. With overall dimensions of 177 mm $\times$ 48.8 mm $\times$ 3.175 mm ($4.8\lambda_0 \times 1.32\lambda_0 \times 0.086\lambda_0$), the antenna array is compact and suitable for satellites with limited surface area. This compact form factor facilitates seamless integration into satellite systems without compromising performance. The proposed antenna is suitable to be employed for the satellite X-band telemetry application extending from 7.9 GHz to 8.4 GHz. A prototype of the proposed antenna has been fabricated and then measured using Vector Network Analyzer (VNA) and anechoic chamber. The proposed antenna's measurement results match the simulated results.

1. INTRODUCTION

The use of X-band technology has been pivotal in enabling high-speed data transmission, large bandwidth, and short-range communication for a wide range of applications. One of the most significant applications of the antenna operating in X-band is satellite telemetry, where it is used for communication between the satellite and the ground station. In particular, the X-band antenna used for telemetry applications operates in the frequency range from 7.9 GHz to 8.4 GHz and with circular polarized performance to ensure reliable communication [1–3]. Despite the significant advancements made in X-band design, X-band antennas that can cater to diverse applications continue to pose a major challenge for researchers. The need for compact, lightweight, and easily integrable antennas in modern communication systems has led to a growing interest in the development of such antennas.

Several antenna designs operating in the X-band satellite applications have been investigated. The first antenna in [1] is a telemetry antenna, covering a bandwidth from 8.025 GHz to 8.4 GHz, with a 3 dB axial ratio bandwidth of 370 MHz, and a maximum gain of 5 dBi. The antenna size is 238 mm ($6.52\lambda_0$) in diameter and 185 mm ($5.13\lambda_0$) in height, which is considered a large size with small gain. The second antenna in [3] is a telemetry circularly polarized antenna for CubeSats, with a bandwidth extending from 8 GHz to 8.4 GHz, a 3 dB axial ratio bandwidth of 400 MHz, and a maximum gain of 5 dBi. The antenna size is $100 \times 100 \times 15$ mm^3 ($2.74\lambda_0 \times 2.74\lambda_0 \times 0.41\lambda_0$). The size of the antenna is relatively big with a large thickness and a small gain. The third antenna in [4] is an enhanced bandwidth X-band microstrip patch antenna, with a bandwidth extending from 10.1 GHz to 11.59 GHz, a maximum gain of 4.3 dBi, and is not circularly polarized. The antenna size is $40 \times 40 \times 1.6$ mm^3 ($145\lambda_0 \times 1.45\lambda_0 \times 0.057\lambda_0$). The fourth antenna in [5] is an X-band slotted substrate integrated waveguide (SIW) antenna with a bandwidth extending from 9.64 GHz to 9.8 GHz, and not circularly polarized, and a maximum gain of 7 dBi. The antenna size is $91.1 \times 50 \times 1.575$ mm^3 ($2.95\lambda_0 \times 162\lambda_0 \times 0.05\lambda_0$). The bandwidth of this antenna is considered narrow, and it does not achieve circular polarization. The fifth antenna in [6] is a leaky-wave antenna based on a substrate integrated waveguide (SIW) with an H-shaped slot array, with a bandwidth extending from 9.9 GHz to 117 GHz and a 3 dB axial ratio bandwidth of 200 MHz extending from 10.3 GHz to 10.5 GHz. The antenna gain fluctuates between 7 dBi and 12 dBi. The antenna size is $310.2 \times 50 \times 1$ mm^3 ($11.16\lambda_0 \times 1.8\lambda_0 \times 0.036\lambda_0$). The antenna size is relatively large, and the gain is not constant along the bandwidth. The antenna is not circularly polarized over the whole bandwidth. The sixth antenna in [7] is an X-band conformal slot antenna array for cube satellite systems, with a bandwidth extending from 9.9 GHz to 10.5 GHz and a maximum gain of 11.15 dBi, and is not circularly polarized. The antenna size is $120 \times 70 \times 3$ mm^3

* Corresponding author: Mostafa Mahmoud Rabie (ad8259@coventry.ac.uk).

($4.08\lambda_0 \times 2.38\lambda_0 \times 0.102\lambda_0$). The seventh antenna in [8] is a corporate-feed substrate integrated waveguide (SIW) slot array antenna, with a bandwidth extending from 9.9 GHz to 10.13 GHz, a 3 dB axial ratio bandwidth of 70 MHz extending from 10.01 GHz to 10.07 GHz, and average gain of 13 dBi. The antenna size is $132.8 \times 23 \times 2.4\,\text{mm}^3$ ($4.43\lambda_0 \times 0.77\lambda_0 \times 0.08\lambda_0$). The bandwidth of this antenna is considered narrow, and the antenna is not circularly polarized over the whole bandwidth. The eighth antenna in [9] is a multi-layered rectangular microstrip antenna, with an inset feeding technique, consisting of a 10 GHz resonating conventional microstrip patch and 9×9 electromagnetic bandgap (EBG) array, with a bandwidth extending from 9.42 GHz to 10.62 GHz, maximum gain of 8.5 dBi, and is not circularly polarized. The antenna size is $55 \times 55 \times 17.67\,\text{mm}^3$ ($1.84\lambda_0 \times 1.84\lambda_0 \times 0.59\lambda_0$). The thickness of the antenna is relatively large.

The evolution of wireless communication systems has led to the development of numerous antenna technologies, each with its unique advantages and limitations. In recent years, substrate integrated waveguide (SIW) antennas and fractal slot antennas have emerged as promising candidates for high-performance, compact, and low-cost antenna design. SIW technology offers several advantages over conventional waveguide technology, such as reduced size, weight, and cost, as well as better integration with other planar circuits [5, 6, 8, 10, 11]. Meanwhile, fractal slot antennas are known for their multiband and wideband characteristics and the ability to achieve circular polarization [12–14]. Circular polarization is a desirable characteristic in many communication systems as it allows for more robust and reliable signal transmission. Fractal slot antennas achieve circular polarization by leveraging the self-similar and iterative nature of fractal geometry. The intricate design of these antennas features a repeating pattern of slots, which creates a highly compact and efficient structure. The fractal geometry allows for multiple resonances at different frequencies, enabling wideband operation [12–14]. By carefully designing the dimensions and arrangements of the slots, fractal slot antennas can generate circularly polarized electromagnetic waves. This unique capability makes them ideal for various applications in wireless communication systems, satellite communication, radar systems, and more.

In this paper, a novel antenna design that combines the benefits of both the SIW and fractal slot technologies is proposed. The proposed antenna is a substrate integrated waveguide (SIW) array with tapered line feeding, which consists of multiple fractal slot elements inside hexagonal ring slot elements arranged in an array configuration. The SIW elements are fed by a tapered microstrip line, which provides a smooth transition from the microstrip line to the substrate integrated waveguide. The array configuration allows us to achieve high gain, high directivity, and low sidelobe levels.

The proposed antenna design will be simulated and analyzed. First, a single element SIW antenna with tapered line feeding will be designed and simulated. Then, the design will be extended to a two-element SIW array antenna and then to a four-element SIW array antenna. Finally, a double-walled four-element SIW array for gain enhancement will be designed and simulated. The double-walled four-element SIW array is fabricated and measured. The fabrication process involved employing advanced manufacturing techniques to ensure precise alignment and accurate replication. Following fabrication, rigorous measurement and characterization were conducted to evaluate the array's performance. The measured results obtained from the experimental setup were then compared to the simulated ones. The performance of the proposed antenna is evaluated in terms of reflection coefficient, axial ratio, gain, radiation pattern, and efficiency.

This paper is organized as follows. Single element SIW with Spidron fractal slot design is presented in Section 2. SIW array realization is presented in Section 3. Experimental results are given in Section 4. Final assessment and comparison with recent X-band antenna designs are introduced in Section 5. Conclusion is presented in Section 6.

2. DESIGN AND ANALYSIS OF A SINGLE ELEMENT SUBSTRATE INTEGRATED WAVEGUIDE (SIW) ANTENNA WITH SPIDRON FRACTAL SLOT AND HEXAGONAL RING SLOT

In this section, the design of a single element substrate integrated waveguide (SIW) with a Spidron fractal slot inside a hexagonal ring slot is introduced, designed, and simulated. The simulation software used is CST studio suite. The antenna is fed by a microstrip tapered feeder for transitioning from microstrip to SIW as shown in Figure 1. The substrate used is Rogers RT-Duroid 5880 with dielectric constant, ε_r of 2.2, and thickness of 3.175 mm. The first design step is a single element substrate integrated waveguide (SIW) with a Spidron fractal slot as shown in Figure 1. In the second design step, a hexagonal ring slot is added for performance enhancement. The hexagonal ring slot contains the Spidron fractal slot inside it as shown in Figure 2.

Step 1: Single element substrate integrated waveguide (SIW) antenna with a Spidron fractal slot.

SIWs are structures that resemble integrated waveguides. They are created by utilizing two sets of conducting cylinders in a dielectric substrate, which connect two parallel metal plates as shown in Figure 3. This design allows the non-planar rectangular waveguide to be transformed into a planar form that can be easily processed using existing planar techniques. The propagation characteristics of SIWs are similar to those of traditional rectangular waveguides. The modes of the SIW align closely with a specific subset of modes found in rectangular waveguides, specifically the TE_{n0} modes where $n = 1, 2$, and so on. Notably, the fundamental mode closely resembles the TE_{10} mode of a rectangular waveguide, with vertical electric current density along the side walls. However, SIWs do not support TM modes due to the presence of gaps between the metal vias. These gaps cause transverse magnetic fields to generate longitudinal surface currents. The presence of these gaps also leads to significant radiation of the longitudinal surface current, thereby preventing the propagation of TM modes. Additionally, SIW structures retain most of the advantages associated with conventional metallic waveguides, such as a high quality-factor and the ability to handle high power [15, 16], and

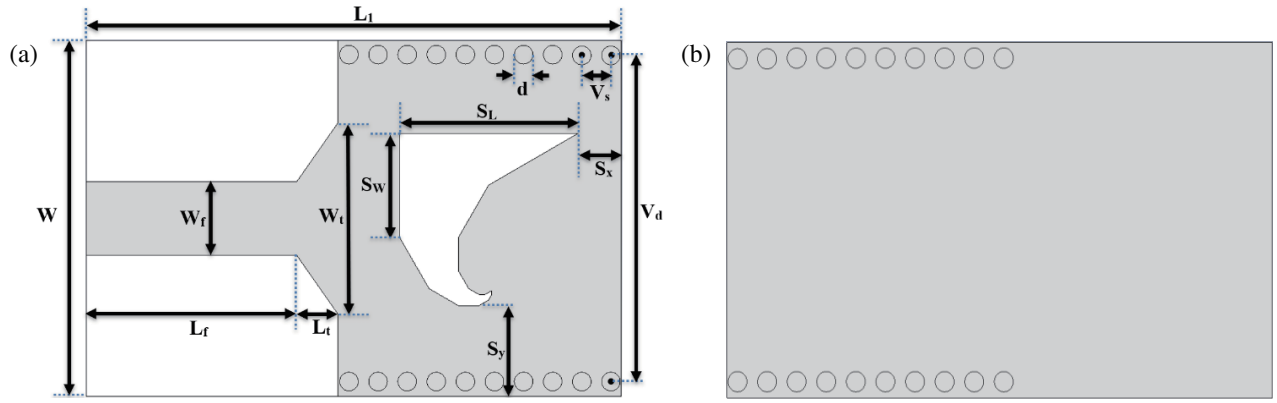

FIGURE 1. Single element substrate integrated waveguide (SIW) antenna with a spidron fractal slot: (a) Front view and (b) Back view.

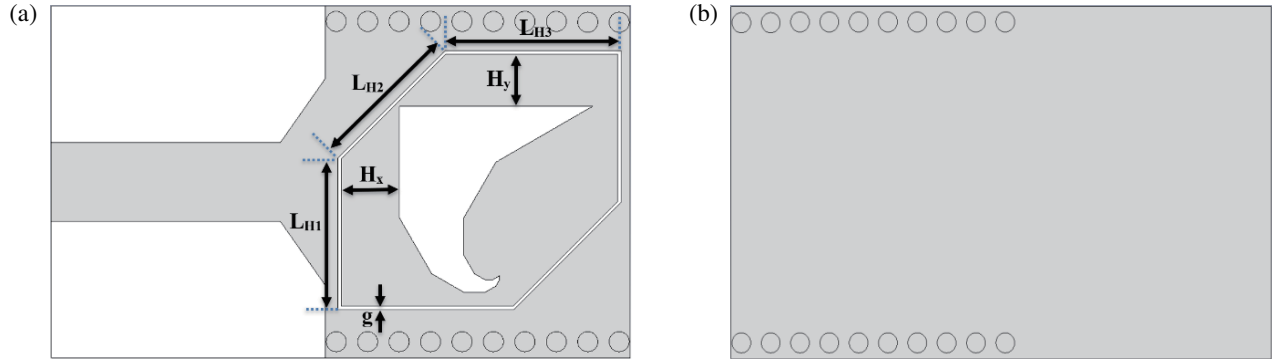

FIGURE 2. Single element substrate integrated waveguide (SIW) antenna with a spidron fractal and hexagonal ring slots: (a) Front view and (b) Back view.

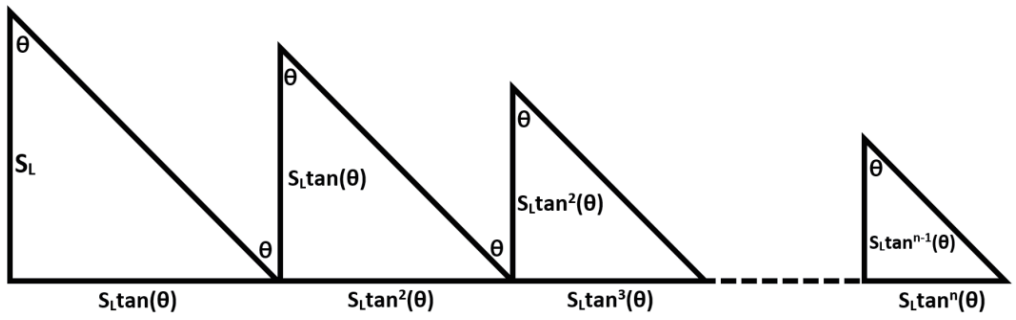

FIGURE 3. Right angle triangles forming the spidron shape.

SIW antenna design usually works in the TE_{10} mode, ($m = 1$, $n = 0$). The parameters, a and a_d at the required resonance frequency, f_r, are calculated in the TE_{10} mode ($m = 1, n = 0$) using the following equations from [15] and [17]:

$$f_r = \frac{c}{2\pi\sqrt{\varepsilon_r}}\sqrt{\left(\frac{m\pi}{a}\right)^2 + \left(\frac{n\pi}{h}\right)^2} \quad (1)$$

$$f_r = \frac{c}{2a} \quad (2)$$

For dielectric field waveguide (DFW), a_d is:

$$a_d = \frac{a}{\sqrt{\varepsilon_r}} \quad (3)$$

$$V_d = a_d + \frac{d^2}{0.95\,(V_s - d)} \quad (4)$$

where c is the speed of light ($c = 3 \times 10^8$), a the total broad side dimension of the rectangular waveguide, and a_d the width of the DFW (Dielectric Filled Waveguide). V_d represents the width of the SIW which is the distance between the two vias rows center to center as shown in Figure 3. The diameter of the via, d, and the spacing between two successive vias, V_s, are determined according to the following conditions [17] and [18]:

$$V_s < 2d \quad (5)$$

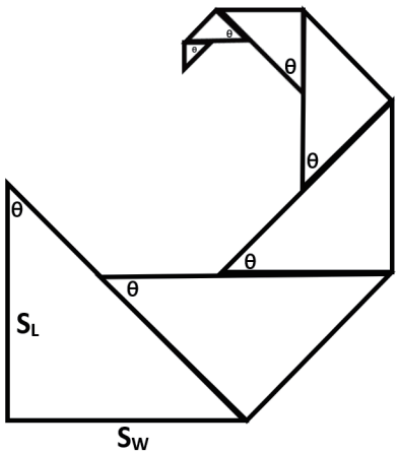

FIGURE 4. Spidron shape.

$$d < \frac{\lambda_g}{5} \tag{6}$$

where λ_g is the guided wavelength and is given by [17]:

$$\lambda_g = \frac{2}{\sqrt{\left(\frac{2\sqrt{\varepsilon_r}}{\lambda}\right)^2 - \left(\frac{1}{V_d}\right)^2}} \tag{7}$$

where λ is the wavelength in free space and is given by:

$$\lambda = \frac{c}{f_r} \tag{8}$$

The slot opening in the SIW structure is selected to be a Spidron fractal slot opening as shown in Figure 1. The selection of a Spidron fractal slot structure in the proposed antenna design stems from the remarkable characteristics exhibited by Spidron fractal antennas. These antennas possess the unique capability to achieve a wide bandwidth while achieving circular polarization within this frequency range. The intricate design of the Spidron fractal slot and its asymmetrical structure allows for enhanced electromagnetic wave interaction, resulting in improved performance and ability to achieve circular polarization [12–14, 19], 20]. A Spidron fractal is composed of a number of right-angle triangles starting with a large triangle with height S_L and then reduced in size by a common factor $\tan(\theta)$ so that the height of the next triangle is $S_L \tan(\theta)$ and so on until reaching the n^{th} triangle whose height would be $S_L \tan^n(\theta)$ as shown in Figure 3 [13]. Each triangle is then rotated backward towards the larger triangle by a fixed angle θ to form the shape of a Spidron as shown in Figure 4. The height of the Spidron slot can be derived starting from the equation of the slot antenna width [15, 21, 22]. The derivation process is outlined as follows:

$$S_W = S_L \tan(\theta) \cong \frac{\lambda_g}{2} \tag{9}$$

$$S_L \cong \frac{\lambda_g}{2\tan(\theta)} \tag{10}$$

$$S_L \cong \frac{C}{2f_r \tan(\theta)\sqrt{\varepsilon_{reff}}} \tag{11}$$

The Spidron fractal slot is placed at distances, S_y, from the bottom side and S_x from the right side of the antenna as shown in Figure 1. The Spidron fractal slot is positioned at the midpoint of the antenna's vertical dimension. The distance S_x is calculated as follows [15]:

$$S_x \cong \frac{\lambda_g}{4} \tag{12}$$

The antenna is fed by a microstrip tapered feeder as shown in Figure 1. Microstrip taper is the most common method for transitioning from microstrip to SIW. Microstrip taper is a gradual transition structure that allows for impedance matching and smooth signal transfer between the microstrip and SIW. It consists of a gradual increase or decrease in the width of the microstrip line to match the characteristic impedance of the SIW. It connects a microstrip of width W_f and the SIW of width V_d, so that both have the same impedance at the desired frequency. The length of the microstrip line is L_f as shown in Figure 1. The length of the taper primarily depends on the variation in width between the microstrip line and SIW. In the millimeter band, where the widths are usually similar for ε_r values ranging from 2 to 10, a taper length of $\lambda_g/4$ is considered appropriate. It is recommended that the taper length be a multiple of $\lambda_g/4$. The taper length L_t and width W_t are calculated as follows [23] and [24]:

$$L_t = \frac{n\lambda g}{4}; \quad n = 1, 2, 3, 4 \ldots \tag{13}$$

$$W_t = W_f + 0.1547 V_d \tag{14}$$

The dimensions of the substrate integrated waveguide (SIW) structure, Spidron fractal slot opening, and microstrip tapered feeder were calculated at the resonance frequency of 8.15 GHz, which corresponds to the center frequency of the required bandwidth for the X-band telemetry application ranging from 7.9 GHz to 8.4 GHz and at angle θ equal to 3 degrees. The calculations were performed considering a dielectric constant, ε_r of 2.2, and substrate thickness, h of 3.175 mm. The overall

TABLE 1. Optimized dimensions.

Parameter	V_d	V_s	d	S_W	S_L	S_x	S_y	L_f	W_f	L_t	W_t	L_1	W	L_{H1}	L_{H2}	L_{H3}	H_x	H_y	g
Value (mm)	39	3.9	2.5	13.8	24	5.5	8.1	27	9.8	5.5	25.5	71	43	17	17	19	7	6.3	0.5

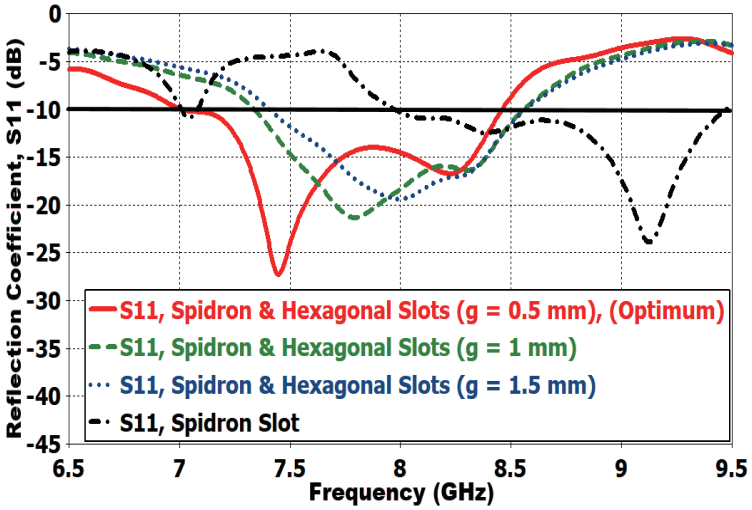

FIGURE 5. Simulated reflection coefficient $|S_{11}|$ of single-element (SIW) antenna with spidron fractal: Comparing performance without hexagonal ring slot and with hexagonal ring slot at $g = 0.5$ mm, 1 mm, and 1.5 mm.

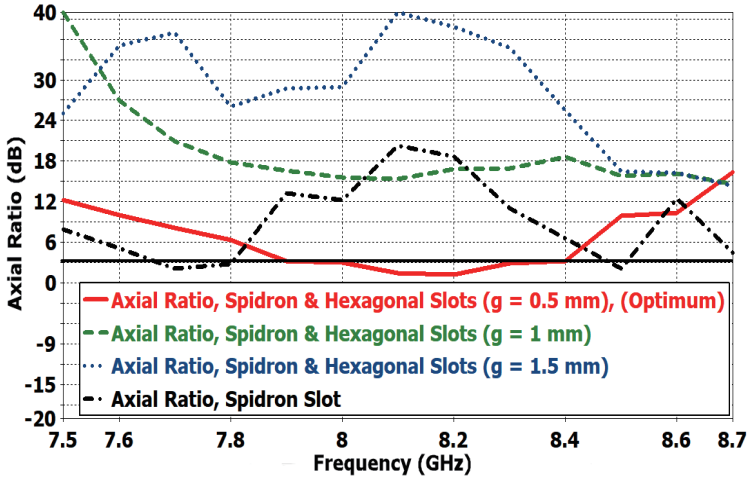

FIGURE 6. Simulated axial ratio (AR)| of single-element (SIW) antenna with spidron fractal: Comparing performance without hexagonal ring slot and with hexagonal ring slot at $g = 0.5$ mm, 1 mm, and 1.5 mm.

length and width of the antenna are L_1 and W respectively as shown in Figure 1. The optimized dimensions are given in Table 1.

The single element substrate integrated waveguide (SIW) antenna with a Spidron fractal slot is then simulated. Figure 5 shows the simulated reflection coefficient $|S_{11}|$. It shows that the antenna resonates in the band extending from 7 GHz to 7.2 GHz and the band extending from 8 GHz to 9.5 GHz. Figure 6 illustrates the simulated axial ratio (AR) for circular polarization, showing a 3-dB AR bandwidth of 170 MHz (from 7.65 GHz to 7.82 GHz). The simulated antenna gain is shown in Figure 7 with a gain that varies between 43 dBi and 75 dBi. It is observed that adjustments are needed to bring the bandwidth within the range of 7.9 GHz to 8.4 GHz for the X-band telemetry application. Additionally, the 3-dB AR bandwidth does not currently match the -10 dB reflection coefficient $|S_{11}|$ bandwidth. To address these issues, a hexagonal ring slot is employed in the next step. This adjustment serves to align the bandwidth with the desired frequency range, widen the 3-dB AR bandwidth, and bring it in line with the -10 dB reflection coefficient $|S_{11}|$ bandwidth.

Step 2: Single element substrate integrated waveguide (SIW) antenna with a Spidron fractal slot and a hexagonal ring slot.

The hexagonal ring slot is introduced to fine-tune the antenna's resonance characteristics. The bandwidth for the X-

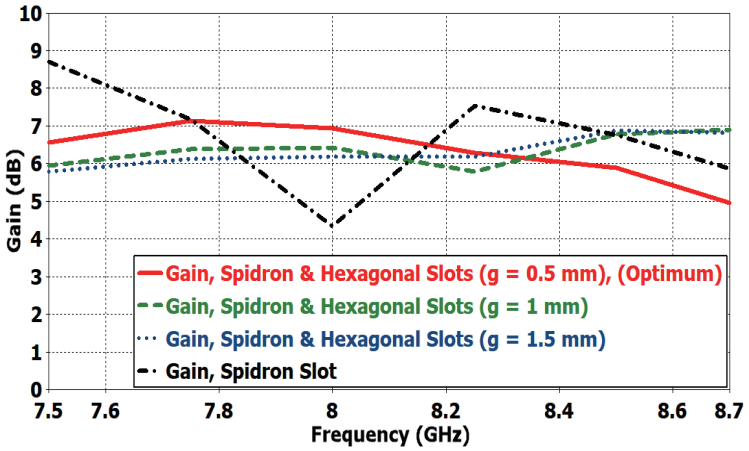

FIGURE 7. Simulated gain of single-element (SIW) antenna with spidron fractal: Comparing performance without hexagonal ring slot and with hexagonal ring slot at $g = 0.5$ mm, 1 mm, and 1.5 mm.

band telemetry application needs to be adjusted to fall within the range of 7.9 GHz to 8.4 GHz. Moreover, the 3-dB AR bandwidth does not match the bandwidth indicated by the -10 dB reflection coefficient $|S_{11}|$. To tackle these problems, a hexagonal ring slot is utilized as shown in Figure 2. This modification aims to synchronize the bandwidth with the desired frequency range, expand the 3-dB AR bandwidth, and align it with the -10 dB reflection coefficient $|S_{11}|$ bandwidth. The hexagonal ring slot is positioned at the precise center of the SIW structure. It is placed at a distance H_x from the left side of the Spidron slot and at a distance H_y from the top side of the Spidron slot, as shown in Figure 2. The hexagonal ring slot has a gap width, g, and outer dimensions of L_{H1}, L_{H2}, and L_{H3} as shown in Figure 2. The outer dimensions are calculated as follows:

$$L_{H1} \cong L_{H2} \cong L_{H3} \cong \frac{\lambda_g}{2} \tag{15}$$

Parametric analyses are performed on the hexagonal ring slot gap width, g, until reaching the optimum results in terms of bandwidth, 3-dB AR bandwidth, and gain. The antenna is simulated at $g = 0.5$ mm, 1 mm and 1.5 mm. The simulated reflection coefficient $|S_{11}|$, AR, and gain are shown in Figure 5, Figure 6, and Figure 7, respectively. The required optimum results are obtained at $g = 0.5$, where the widest bandwidth is achieved extending from 7 GHz to 8.44 GHz, and the antenna is circularly polarized in the required band with a 3-dB AR bandwidth extending from 7.9 GHz to 8.4 GHz. Additionally, at $g = 0.5$ the antenna's gain varies between 6 dBi and 7.1 dBi within the required frequency band (7.9 GHz–8.4 GHz). The optimized dimensions of the SIW antenna with a Spidron fractal slot and a hexagonal ring slot are given in Table 1.

For circular polarization mechanism justification, Figure 8 illustrates the simulated surface current at a frequency of 8.15 GHz. The distribution of surface current in an antenna plays a crucial role in determining its radiation properties. The four subfigures in Figure 8, namely (a), (b), (c), and (d), depict the surface current distribution at phase angles of 0, 90, 180, and 270 degrees, respectively. The maximum surface current observed is 62.7 A/m. The total surface current, denoted as J_T, represents the combined vector sum of all significant surface current distributions at each phase. Notably, the magnitudes of the total surface current, J_T, at 0 and 90 degrees are equal, but they have opposite directions compared to the total surface current at 180 and 270 degrees. Additionally, the total surface current, J_T, direction rotates in a clockwise manner when comparing each phase with the previous one. Consequently, this generates left-hand circularly polarized (LHCP) radiation in the positive z direction, which corresponds to the front side of the antenna. The simulated radiation patterns of E-plane (phi $= 0°$) and H-plane (phi $= 90°$) at frequency of 8.15 GHz are shown in Figures 9(a) and (b), respectively.

3. SIW ARRAY REALIZATION

In this section, we present the realization of a slot array from a single element to achieve gain enhancement. As the number of slot elements increases, the gain of the array increases [25, 26]. Initially, a two-element (2×1) substrate integrated waveguide (SIW) array is introduced, demonstrating improved gain compared to a single element. Building upon this, a four-element (4×1) SIW array is then presented, showcasing further gain enhancement. Additionally, a double-walled SIW array is introduced, aiming to achieve even higher levels of gain. The introduction of the double-walled structure provides additional opportunities for gain enhancement in SIW arrays.

3.1. Two Elements SIW Array

In this subsection, a (2×1) SIW array is realized, where a second (Spidron fractal slot and a hexagonal ring slot) element is added to the SIW structure for gain enhancement as shown in Figure 10. For the SIW array the separation, E_s, between two successive elements is the distance between two successive Spidron-fractal slots as shown in Figure 10. The separation distance, E_s, is calculated as follows:

$$E_s \cong \frac{\lambda_g}{2} \tag{16}$$

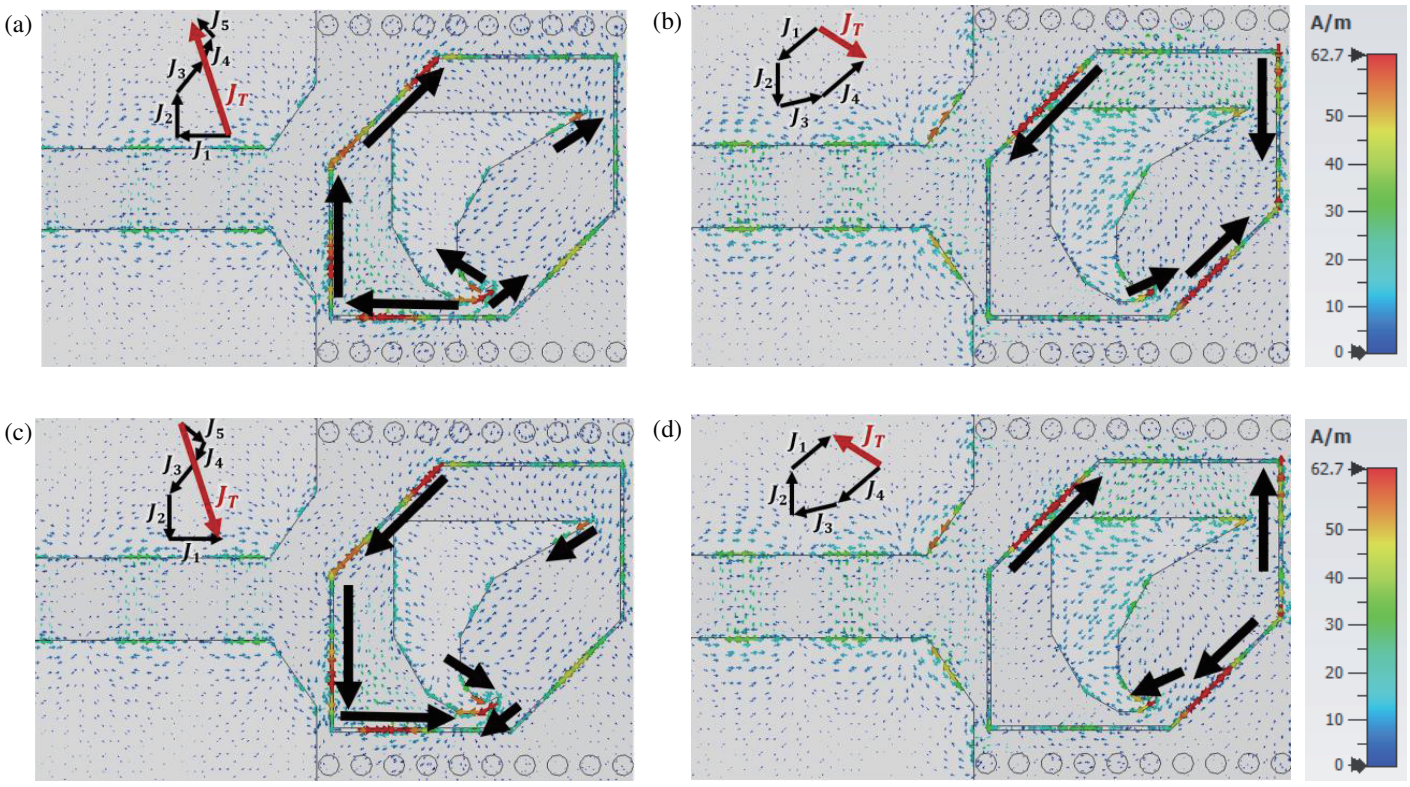

FIGURE 8. Simulated surface current distribution at 8.15 GHz of the Single element substrate integrated waveguide (SIW) antenna with a spidron fractal slot and a hexagonal ring slot: (a) °, (b) 90°, (c) 180°, (d) 270°.

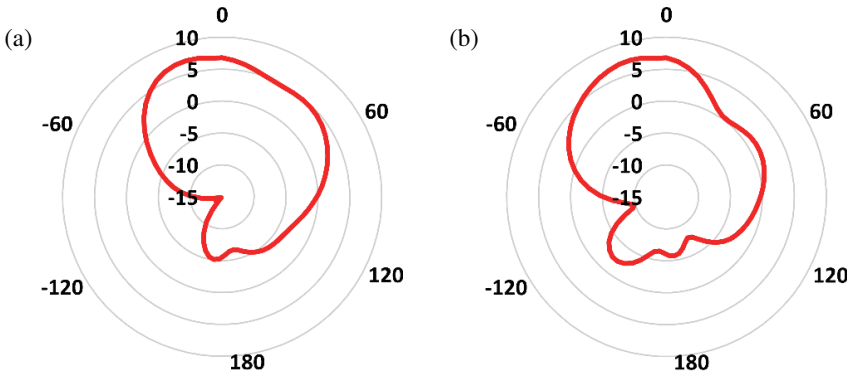

FIGURE 9. Simulated radiation pattern at 8.15 GHz of the Single element substrate integrated waveguide (SIW) antenna with a spidron fractal slot and a hexagonal ring slot: (a) E-plane (phi $= 0°$), (b) H-plane (phi $= 90°$).

The simulated reflection coefficient $|S_{11}|$ is shown in Figure 13. The two elements SIW array achieved a bandwidth of 1.22 GHz extending from 7.2 GHz to 8.42 GHz. The two elements SIW array is circularly polarized with a 3-dB AR bandwidth of 750 MHz extending from 7.9 GHz to 8.65 GHz as shown in Figure 14. The two elements SIW array achieved a maximum gain of 8.5 dBi as shown in Figure 15. The gain is increased by 19.72% compared to the gain of the single element SIW. The simulated radiation patterns of E-plane (phi $= 0°$) and H-plane (phi $= 90°$) of the two elements SIW array at frequency of 8.15 GHz are shown in Figures 16(a) and (b), respectively. The overall length and width of the two elements SIW array are L_2 and W respectively as shown in Figure 10. The optimized values of the separation distance, E_s, and the length, L_2, of the two elements SIW array are given in Table 2.

3.2. Four Elements SIW Array

In this subsection, a (4×1) SIW array is realized, where two more (Spidron fractal slot and a hexagonal ring slot) elements are added to the two elements SIW array as shown in Figure 11 for further gain enhancement. The simulated reflection coefficient $|S_{11}|$ is shown in Figure 13. The four elements SIW array achieved a bandwidth of 1.2 GHz extending from 7.25 GHz to 8.45 GHz. The four elements SIW array is circularly polar-

TABLE 2. Optimized dimensions for the double-walled four elements SIW array.

Parameter	Value (mm)
E_s	11.9
L_2	108
L_3	177
W_E	48.8

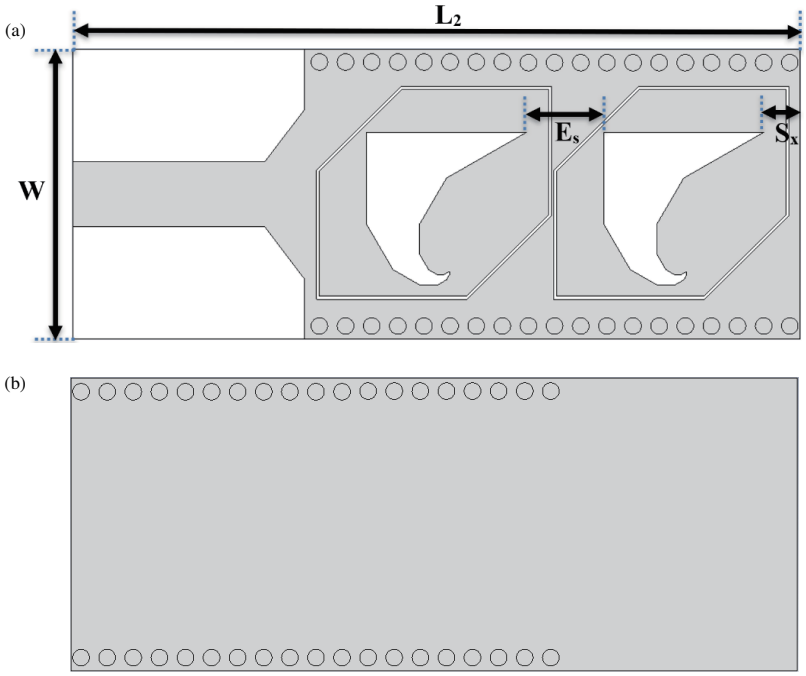

FIGURE 10. Two elements SIW array: (a) Front view and (b) Back view.

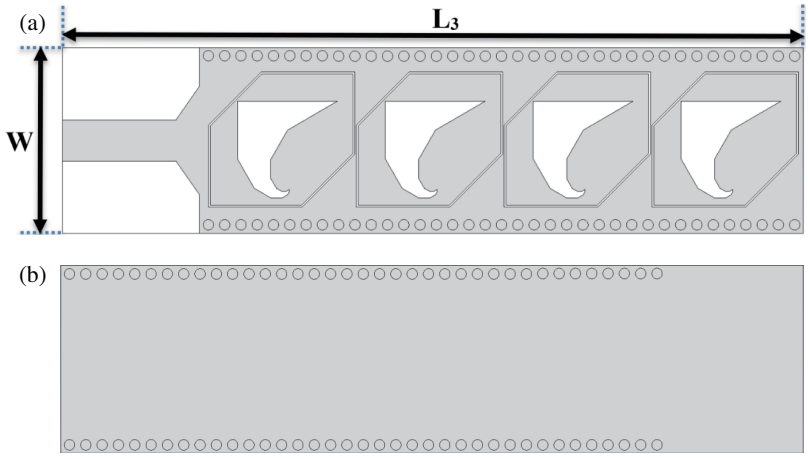

FIGURE 11. Four elements SIW array: (a) Front view and (b) Back view.

ized with a 3-dB AR bandwidth of 720 MHz extending from 7.88 GHz to 8.62 GHz as shown in Figure 14. The four elements SIW array achieved a maximum gain of 10.2 dBi as shown in Figure 15. The gain is increased by 20% compared to the gain of the two elements SIW array. The simulated radiation patterns of E-plane (phi $= 0°$) and H-plane (phi $= 90°$) of the four elements SIW array at frequency of 8.15 GHz are shown in Figures 16(a) and (b), respectively. The overall length and width of the four elements SIW array are L_3 and W respectively as shown in Figure 11. The optimized value of the length, L_3, of the four elements SIW array is given in Table 2.

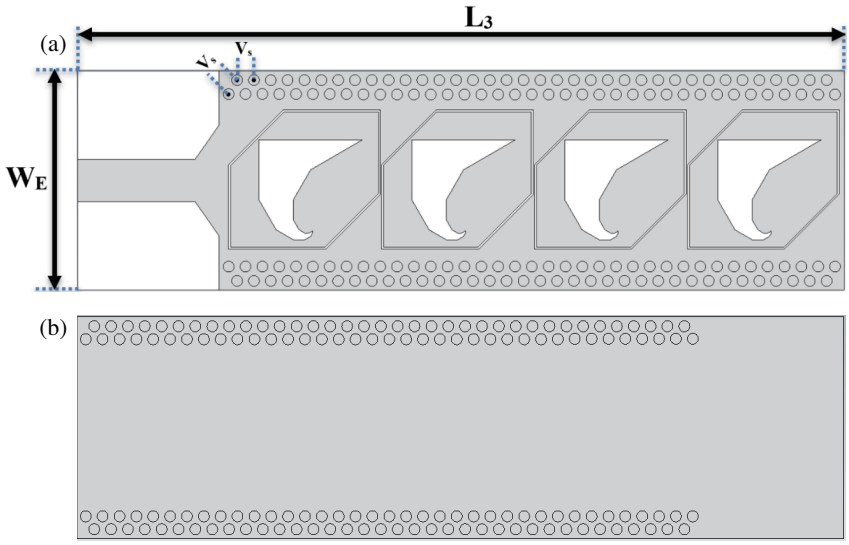

FIGURE 12. Double-walled four elements SIW array: (a) Front view and (b) Back view.

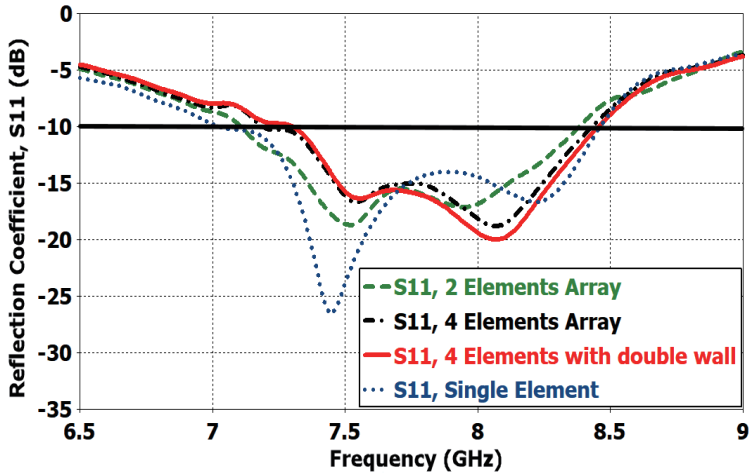

FIGURE 13. Simulated reflection coefficient $|S_{11}|$ of single element, two elements array, four elements array and four elements with double-wall array.

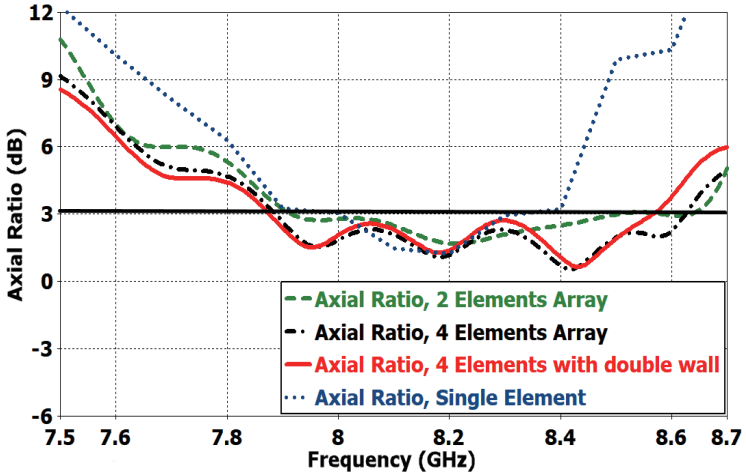

FIGURE 14. Simulated axial-ratio (AR) of single element, two elements array, four elements array and four elements with double-wall array.

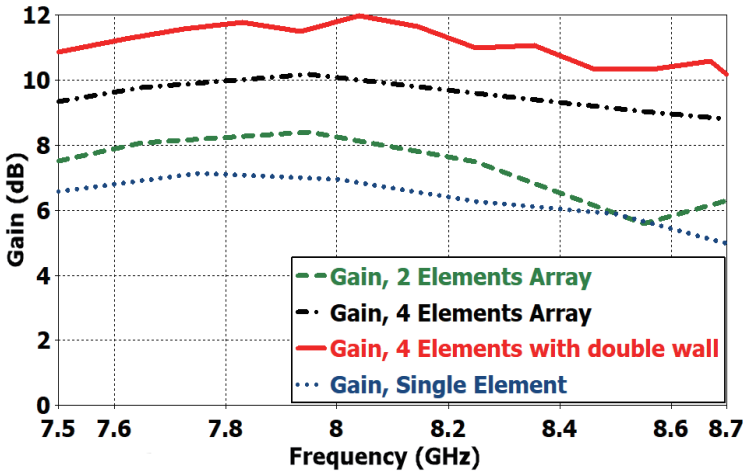

FIGURE 15. Simulated gain of single element, two elements array, four elements array and four elements with double-wall array.

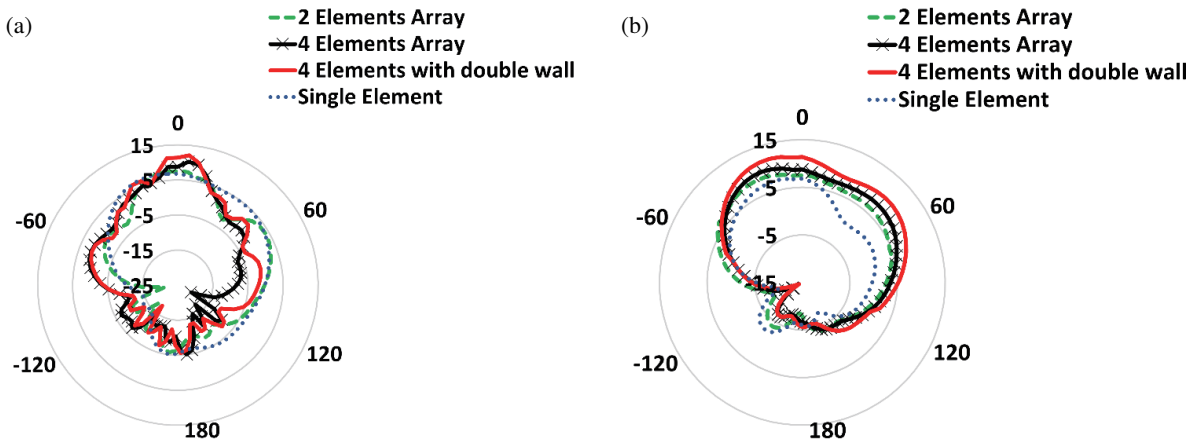

FIGURE 16. Simulated radiation patterns at 8.15 GHz of single element, two elements array, four elements array and four elements with double-wall array: (a) E-plane (phi $= 0°$), (b) H-plane (phi $= 90°$).

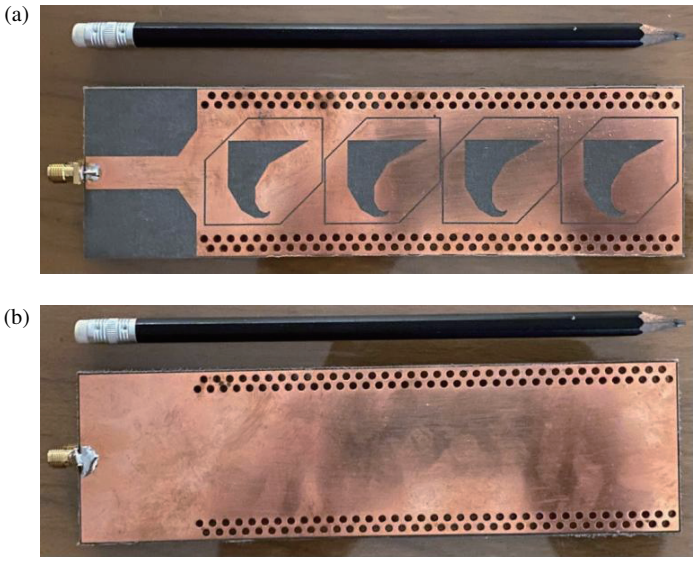

FIGURE 17. Fabricated double-walled four elements SIW array: (a) Front view. (b) Back view.

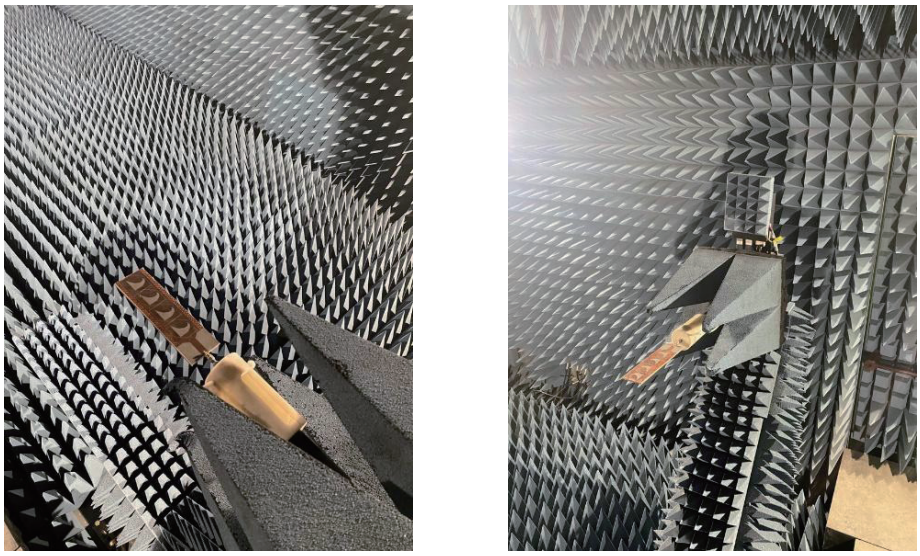

FIGURE 18. Fabricated double-walled four elements SIW array measurement in the anechoic chamber.

3.3. Double-Walled Four Elements SIW Array

In this subsection, an extra vias line is added to the top and bottom sides of the four elements SIW array making it a double-walled four elements SIW array as shown in Figure 12. The utilization of a double-walled substrate-integrated waveguide (SIW) structure offers substantial improvements in gain compared to a single-walled SIW [11]. The first via in the added vias-line (wall) is placed mid-distance between the first and second vias in the below vias-line (wall) with a center-to-center distance, V_s, between it and the first or second vias in the below vias-line (wall) as shown in Figure 12. The center-to-center distance between two successive vias in the added vias-line (wall) is equal to V_s as shown in Figure 12. The simulated reflection coefficient $|S_{11}|$ is shown in Figure 13. The double-walled four elements SIW array achieved a bandwidth of 1.21 GHz extending from 7.25 GHz to 8.46 GHz. After comparing the reflection coefficients $|S_{11}|$ of the single element, two elements, four elements, and double-walled four elements antennas, it is observed that differences occur as shown in Figure 13. When converting a single element to an array (two or four elements) and also when extra vias-lines are added to the top and bottom sides of the four elements antenna array, the structure or configuration of the overall antenna is essentially changed. This change can introduce new effects such as mutual coupling between the elements and impedance mismatches. These effects can cause slight variations in the reflection coefficient $|S_{11}|$. However, the single element, two elements, four elements, and double-walled four elements antennas managed to achieve the required bandwidth for the required application.

The double-walled four elements SIW array is circularly polarized with a 3-dB AR bandwidth of 710 MHz extending from 7.87 GHz to 8.58 GHz as shown in Figure 14. The double-walled four elements SIW array achieved a maximum gain of 12 dBi as shown in Figure 15. The gain is increased by 17.6% compared to the gain of the four elements SIW array. The simulated radiation patterns of E-plane (phi $=$ 0°) and H-plane (phi $=$ 90°) of the double-walled four elements SIW array at frequency of 8.15 GHz are shown in Figures 16(a) and (b), respectively. The overall length and width of the double-walled four elements SIW array are L_3 and W_E respectively as shown in Figure 12. The optimized value of the width, W_E, of the double-walled four elements SIW array is given in Table 2.

4. EXPERIMENTAL RESULTS

The proposed double-walled four elements SIW antenna array is fabricated using an RT/Duroid 5880 substrate with dielectric constant, $\varepsilon_{\mathrm{r}} = 2.2$, low loss tangent $\tan(\delta) = 0.0009$, and height $h = 3.175$ mm as shown in Figure 17. The antenna's simulated radiation patterns and antenna parameters are presented, as well as the measurements taken from a fabricated prototype of the antenna. The reflection coefficient $|S_{11}|$ of the antenna is measured using ROHDE & SCHARZ 20 Vector Network Analyzer (VNA). The radiation pattern and other antenna parameters are then measured in an anechoic chamber as shown in Figure 18. Simulated and measured radiation patterns and antenna parameters of the double-walled four elements SIW antenna array are analyzed and compared. The radiation patterns of E-plane (phi $=$ 0) and H-plane (phi $=$ 90) at frequency of 8.15 GHz for the simulated and fabricated antennas are shown in Figures 19(a) and (b), respectively. The radiation pattern of the double-walled four elements SIW antenna array is similar to the radiation patterns of the satellite X-band antenna designs in [27–30] proving its suitability for X-band satellite applications. The simulated and measured reflection coefficients $|S_{11}|$ are shown in Figure 2 with -10 dB reflection coefficient $|S_{11}|$ bandwidths of 121 GHz extending from 7.25 GHz to 8.46 GHz and 15 GHz extending from 7 GHz to 8.5 GHz, respectively. The simulated and measured axial ratios are shown in Figure 21 indicating that the antenna is circularly polarized in the required band. The simulated and measured AR 3-dB bandwidths are 710 MHz extending from 7.87 GHz to 8.58 GHz and 81 MHz extending from 78 GHz to 8.61 GHz,

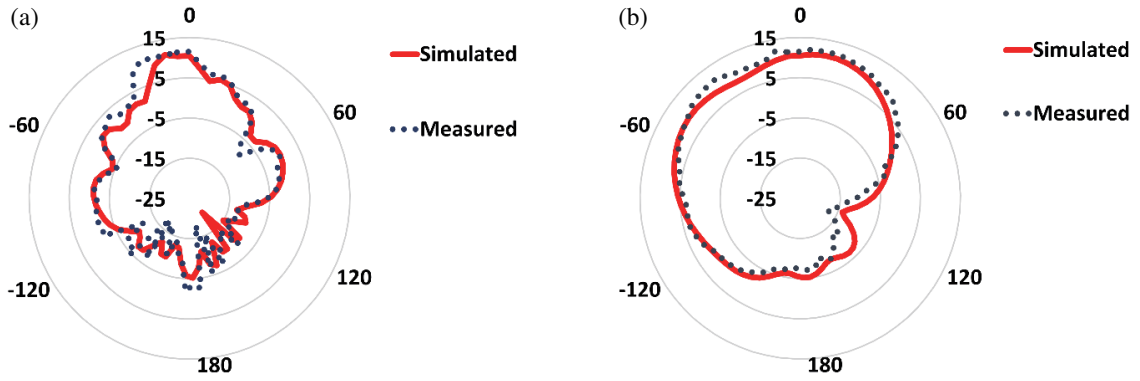

FIGURE 19. Simulated and measured radiation patterns at 815 GHz of the double-walled four elements SIW array: (a) E-plane (phi $= 0°$), (b) H-plane (phi $= 90°$).

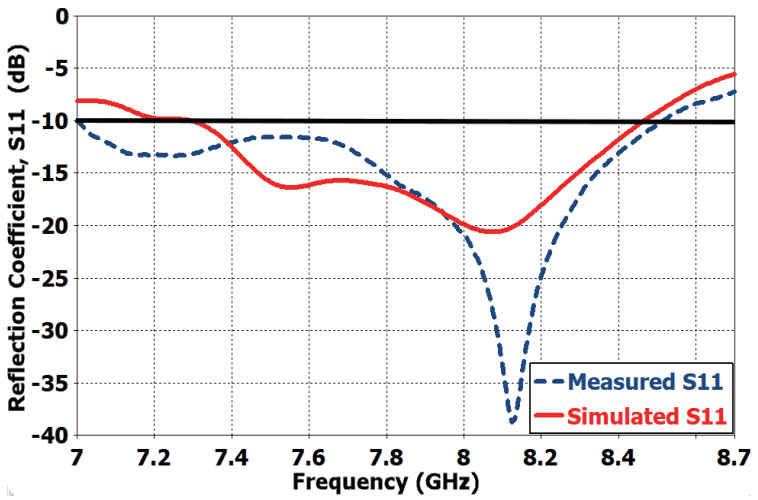

FIGURE 20. Measured vs simulated reflection coefficient $|S_{11}|$ of the double-walled four elements SIW array.

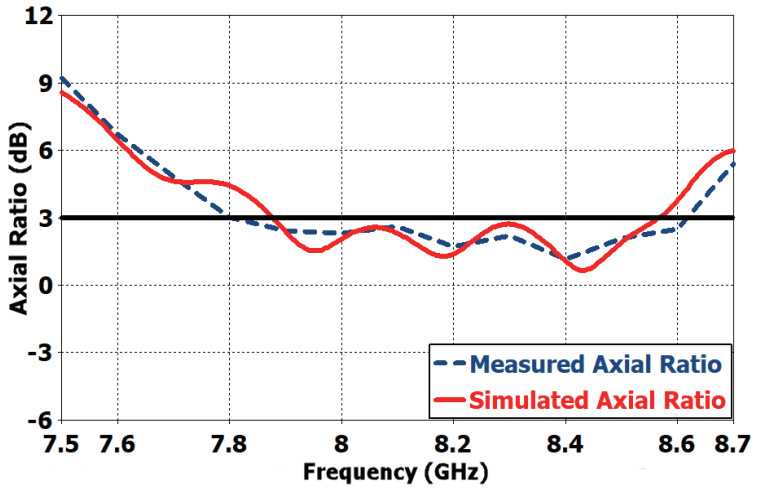

FIGURE 21. Measured vs simulated axial ratio (AR) of the double-walled four elements SIW array.

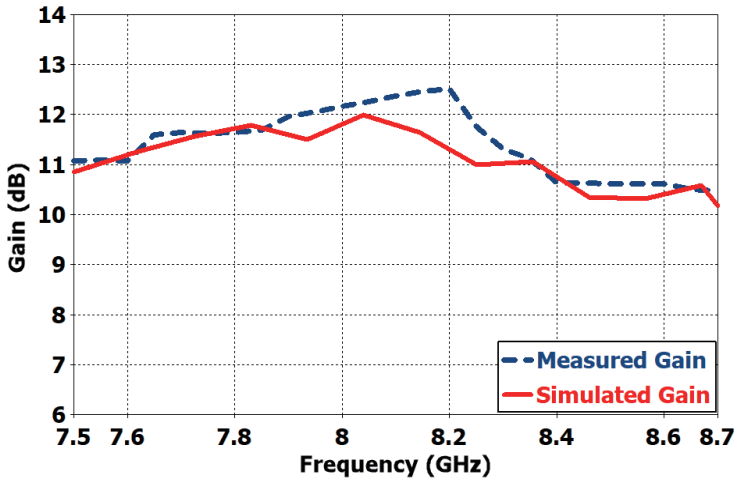

FIGURE 22. Measured vs simulated gain of the double-walled four elements SIW array.

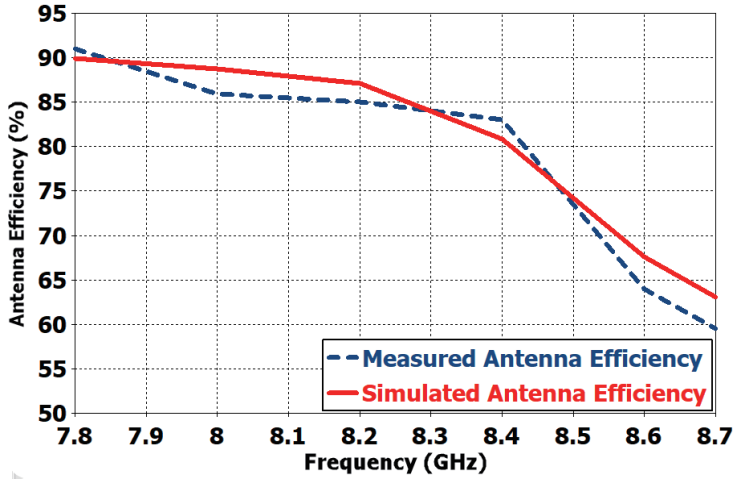

FIGURE 23. Measured vs simulated antenna efficiency of the double-walled four elements SIW array.

respectively. The simulated and measured gains are shown in Figure 22 with maximum gains of 12 dBi and 12.51 dBi, respectively. The simulated and measured total efficiencies are shown in Figure 23 with maximum efficiencies of 89% and 89.5%, respectively. It is obvious that the antenna efficiency drops at frequencies higher than 8.46 GHz, because the antenna is not matched for frequencies higher than 8.46 GHz and 8.5 GHz for the simulated and measured antenna efficiencies respectively as shown in Figure 20. This indicates that the proposed antenna design is well optimized and capable of achieving excellent performance in terms of efficient use of the available power. The results demonstrate that the measured parameters and radiation patterns of the fabricated antenna match the simulation results, achieving the desired design requirements.

5. FINAL ASSESSMENT AND COMPARISON WITH RECENT X-BAND ANTENNA DESIGNS

This section presents a comprehensive comparison of the proposed "Circularly Polarized SIW Fractal Slot Antenna Array for X-Band Satellite Applications" with several recent X-band antenna designs as given in Table 3. The proposed antenna operates within the frequency range extending from 7 GHz to 8.5 GHz, with a 3-dB axial ratio bandwidth of 810 MHz extending from 7.8 GHz to 8.61 GHz and a maximum gain of 12.51 dBi. The physical dimensions of the antenna are specified as 177 mm $\times$ 48.8 mm $\times$ 3.175 mm ($4.8\lambda_0 \times 1.32\lambda_0 \times 0.086\lambda_0$), where λ_0 represents the free-space wavelength at the center frequency. The performance of this work is compared with the referenced antenna designs, indicating that the proposed antenna exhibits a higher maximum gain of 12.51 dBi, surpassing the gains achieved by most of the other designs. Furthermore, the 3-dB axial ratio bandwidth of 810 MHz demonstrates improved circular polarization characteristics, outperforming several previous designs that were not circularly polarized or had narrower bandwidths. The antenna size of 177 mm $\times$ 48.8 mm $\times$ 3.175 mm also represents a compact form factor, offering potential advantages in terms of integration and deployment.

Overall, the results of this assessment highlight the promising performance of the circularly polarized SIW fractal slot antenna array for X-band satellite applications. The higher gain, wider axial ratio bandwidth, and compact size make it a

TABLE 3. Comparison with some recent designs of X-band antennas.

Reference	Bandwidth (Hz)	Axial Ratio 3 dB Bandwidth (Hz)	Maximum Gain (dBi)	Antenna Size (mm^3)
[1]	8.025–8.4 GHz (370 MHz)	8.025–8.4 GHz (370 MHz)	5 dBi	Diameter: 238 mm ($6.52\lambda_0$) Height: 185 mm ($5.13\lambda_0$)
[3]	8–8.4 GHz (400 MHz)	8–8.4 GHz (400 MHz)	5 dBi	(Length × Width × Height): 100 mm × 100 mm × 15 mm ($2.74\lambda_0 \times 2.74\lambda_0 \times 0.41\lambda_0$)
[5]	9.64–9.8 GHz (160 MHz)	Not circularly polarized	7 dBi	(Length × Width × Height): 91.1 mm × 50 mm × 1.575 mm ($2.95\lambda_0 \times 1.62\lambda_0 \times 0.05\lambda_0$)
[6]	9.9–11.7 GHz (1.8 GHz)	10.3–10.5 GHz (200 MHz)	9.5 dBi	(Length × Width × Height): 310.2 mm × 50 mm × 1 mm ($11.16\lambda_0 \times 1.8\lambda_0 \times 0.036\lambda_0$)
[7]	9.9–10.5 GHz (600 MHz)	Not circularly polarized	11.15 dBi	(Length × Width × Height): 120 mm × 70 mm × 3 mm ($4.08\lambda_0 \times 2.38\lambda_0 \times 0.102\lambda_0$)
[8]	9.9–10.13 GHz (230 MHz)	10.01–10.07 GHz (70 MHz)	13 dBi	(Length × Width × Height): 132.8 mm × 23 mm × 2.4 mm ($4.43\lambda_0 \times 0.77\lambda_0 \times 0.08\lambda_0$)
[9]	9.42–10.62 GHz (1.2 GHz)	Not circularly polarized	8.5 dBi	(Length × Width × Height): 55 mm × 55 mm × 17.67 mm ($1.84\lambda_0 \times 1.84\lambda_0 \times 0.59\lambda_0$)
This work	7–8.5 GHz (1.5 GHz)	7.8–8.61 GHz (810 MHz)	12.51 dBi	(Length × Width × Height): 177 mm × 48.8 mm × 3.175 mm ($4.8\lambda_0 \times 1.32\lambda_0 \times 0.086\lambda_0$)

compelling choice for various X-band communication systems, where efficient circularly polarized antennas are desired. Further investigations and practical implementations of this design can contribute to the advancements in satellite communication technology.

6. CONCLUSION

In this paper, a circularly polarized double-walled substrate integrated waveguide (SIW) fractal slot antenna array for X-band satellite applications is designed simulated, fabricated, and tested. The single element SIW antenna design is introduced and analyzed. The realizations of two elements and four elements antenna array are introduced. The realization of double-walled SIW four elements array for gain enhancement is introduced. The proposed double-walled SIW four elements antenna array achieved a bandwidth of 15 GHz, covering the X-band frequency range from 7 GHz to 8.5 GHz. It achieved circular polarization with an axial ratio (AR) 3-dB bandwidth of 810 MHz, ranging from 7.8 GHz to 8.61 GHz. It is suitable for satellite X-band telemetry application. The achieved gain of the proposed double-walled SIW four elements antenna array varies between 11 dBi and 12.51 dBi. Its final overall dimensions are $177 \times 48.8 \times 3.175\ mm^3$, making it suitable for satellites with limited surface area. The total antenna efficiency reaches 89%. This suggests that the proposed antenna design is well tuned and can accomplish an outstanding performance. The effectiveness of the design approach was confirmed by conducting measurements on an actual prototype, which provided additional evidence of its reliability.

REFERENCES

[1] Arnaud, E., J. Dugenet, K. Elis, A. Girardot, D. Guihard, C. Menudier, T. Monediere, F. Roziere, and M. Thevenot, "Compact isoflux X-band payload telemetry antenna with simultaneous dual circular polarization for LEO satellite applications," *IEEE Antennas and Wireless Propagation Letters*, Vol. 19, No. 10, 1679–1683, Oct. 2020.

[2] Leszkowska, L., M. Rzymowski, K. Nyka, and L. Kulas, "High-gain compact circularly polarized X-band superstrate antenna for CubeSat applications," *IEEE Antennas and Wireless Propagation Letters*, Vol. 20, No. 11, 2090–2094, Nov. 2021.

[3] Fouany, J., M. Thevenot, E. Arnaud, F. Torres, C. Menudier, T. Monediere, and K. Elis, "New concept of telemetry X-band circularly polarized antenna payload for CubeSat," *IEEE Antennas and Wireless Propagation Letters*, Vol. 16, 2987–2991, 2017.

[4] Islam, M. M., M. T. Islam, M. R. I. Faruque, and W. Hueyshin, "Design of an X-band microstrip patch antenna with enhanced bandwidth," in *2013 2nd International Conference on Advances in Electrical Engineering (ICAEE)*, 313–317, Dkaka, Bangladesh, 2013.

[5] Zeba, F. and S. Mohanty, "X-band slot antenna based on substrate integrated waveguide transmission technique," *International Journal of Engineering Research & Technology (IJERT)*, Vol. 7, No. 2, 290–293, 2018.

[6] Liu, J., X. Tang, Y. Li, and Y. Long, "Substrate integrated waveguide leaky-wave antenna with H-shaped slots," *IEEE Transactions on Antennas and Propagation*, Vol. 60, No. 8, 3962–3967, Aug. 2012.

[7] Khalil, H., M. M. Ahmed, and U. Rafique, "X-band conformal antenna array for low cost cubesats," in *2018 International Conference on Innovation and Intelligence for Informatics, Computing, and Technologies (3ICT)*, Sakhier, Bahrain, 2018.

[8] Elahi, Amn-e A. and P. Rezaei, "SIW corporate-feed network for circular polarization slot array antenna," *Wireless Personal Communications*, Vol. 111, 2129–2136, 2020.

[9] Gaharwar, M. and D. C. Dhubkarya, "X-band multilayer stacked microstrip antenna using novel electromagnetic band-gap structures," *IETE Journal of Research*, Vol. 69, No. 4, 2015–2024, 2023.

[10] Maged, M. A., F. El-Hefnawi, H. M. Akah, A. El-Akhdar, and H. El-Hennawy, "Design and realization of circular polarized SIW slot array antenna for cubesat intersatellite links," *Progress In Electromagnetics Research Letters*, Vol. 77, 81–88, 2018.

[11] Anand, S. and D. Rokhini, "A double line SIW cavity backed antenna for WLAN applications," *International Journal of RF and Microwave Computer-Aided Engineering*, Vol. 29, No. 9, e21861, 2019.

[12] Karmakar, A., "Fractal antennas and arrays: A review and recent developments," *International Journal of Microwave and Wireless Technologies*, Vol. 13, No. 2, 173–197, 2021.

[13] Kwon, O. H., W. B. Park, S. Lee, J. M. Lee, Y. M. Park, and K. C. Hwang, "3D-printed super-wideband spidron fractal cube antenna with laminated copper," *Applied Sciences*, Vol. 7, No. 10, 979, 2017.

[14] Nguyen Thi, T., K. C. Hwang, and H. B. Kim, "Dual-band circularly-polarised Spidron fractal microstrip patch antenna for Ku-band satellite communication applications," *Electronics Letters*, Vol. 49, No. 7, 444–445, 2013.

[15] Moitra, S., A. K. Mukhopadhyay, and A. K. Bhattacharjee, "Ku-band substrate integrated waveguide (SIW) slot array antenna for next generation networks," *Global Journal of Computer Science and Technology Network, Web & Security*, Vol. 13, No. 5, 2013.

[16] Deslandes, D. and K. Wu, "Accurate modeling, wave mechanisms, and design considerations of a substrate integrated waveguide," *IEEE Transactions on Microwave Theory and Techniques*, Vol. 54, No. 6, 2516–2526, 2006.

[17] Rayas-Sanchez, J. E. and V. Gutierrez-Ayala, "A general EM-based design procedure for single-layer substrate integrated waveguide interconnects with microstrip transitions," in *2008 IEEE MTT-S International Microwave Symposium Digest*, Atlanta, GA, USA, 2008.

[18] Wu, K., D. Deslandes, and Y. Cassivi, "The substrate integrated circuits-a new concept for high-frequency electronics and optoelectronics," in *6th International Conference on Telecommunications in Modern Satellite, Cable and Broadcasting Service, 2003. TELSIKS 2003*, Nis, Yugoslavia, 2003.

[19] Trinh-Van, S., H. B. Kim, G. Kwon, and K. C. Hwang, "Circularly polarized spidron fractal slot antenna arrays for broadband satellite communications in ku-band," *Progress In Electromagnetics Research*, Vol. 137, 203–218, 2013.

[20] Altaf, A., Y. Yang, K.-Y. Lee, and K. C. Hwang, "Wideband circularly polarized spidron fractal slot antenna with an embedded patch," *International Journal of Antennas and Propagation*, Vol. 2017, 1–7, 2017.

[21] Sun, X.-b., M.-y. Cao, J.-j. Hao, and Y.-j. Guo, "A rectangular slot antenna with improved bandwidth," *AEU-International Journal of Electronics and Communications*, Vol. 66, No. 6, 465–466, 2012.

[22] Balanis, C. A., *Antenna Theory: Analysis and Design*, 4th ed., John Wiley & Sons, 2016.

[23] Maruti, A. M. and B. S. N. Kishore, "Dual-band SIW slot array filtering antenna for X and Ku band applications," *Progress In Electromagnetics Research Letters*, Vol. 103, 109–117, 2022.

[24] Kordiboroujeni, Z. and J. Bornemann, "New wideband transition from microstrip line to substrate integrated waveguide," *IEEE Transactions on Microwave Theory and Techniques*, Vol. 62, No. 12, 2983–2989, Dec. 2014.

[25] Touhami, N. A., T. Elhamadi, M. A. Ennasar, *et al.*, "High-gain and broadband SIW cavity-backed slots antenna for X-band applications," *International Journal of Microwave and Wireless Technologies*, Vol. 13, No. 10, 1078–1085, 2021.

[26] Bharath, K., S. V. Nandigama, D. RamaKrishna, and V. M. Pandharipande, "High performance millimeter wave SIW slotted array antenna," *Progress In Electromagnetics Research C*, Vol. 125, 15–23, 2022.

[27] Anim, K., P. Danuor, S.-O. Park, and Y.-B. Jung, "High-efficiency broadband planar array antenna with suspended microstrip slab for X-band SAR onboard small satellites," *Sensors*, Vol. 22, No. 1, 252, 2022.

[28] Nunna, B. A. and V. K. Kothapudi, "Design and analysis of 1×4 corporate feed conformal microstrip antenna array for X-band spaceborne synthetic aperture radar applications," in *Advances in Signal Processing, Embedded Systems and IoT*, 93–102, 2023.

[29] Abouelnaga, T. G., M. B. Tayel, and A. F. Desouky, "High gain UWB four elements antenna array for C-band and X-band application," *Open Journal of Antennas and Propagation*, Vol. 8, No. 2, 19–29, 2020.

[30] Genovesi, S. and F. A. Dicandia, "Characteristic modes analysis of a near-field polarization-conversion metasurface for the design of a wideband circularly polarized X-band antenna," *IEEE Access*, Vol. 10, 88 932–88 940, 2022.